A Three-Phase Overlapping Winding–Based Wireless Charging System for Transportation Applications

Samir Chowdhury, *Member, IEEE*, Md Tawhid Bin Tarek, *Student Member, IEEE*, Md Ehsanul Haque, *Member, IEEE*, and Yilmaz Sozer, *Fellow, IEEE*

***Abstract*—This article proposes a two-layer overlapping winding–based three-phase wireless vehicle charging system with a coil span of 180°. This coil structure offers higher coupling and balance inductance matrices between the transmitter and receiver and improves system efficiency. The system performance improvement has been validated through detailed analysis and simulation results and compared with the benchmark for the same electrical parameters, air gap, and coil volume. Finite element analysis–based simulation results were presented for a 7.7-kW wireless power transfer (WPT) over a 200-mm air gap. An experimental prototype of the proposed system is developed operating at the resonant frequency of 86 kHz with a 200-mm air gap between the coils to validate the design. Both the simulation and experimental results showed a significant increase in efficiency and coupling compared to the conventional WPT systems.**

***Index Terms*—Electric vehicles (EVs), electromagnetic coupling, resonance, wireless charging, wireless power transmission (WPT).**

I. Introduction

IN RECENT times, most hybrid and electric vehicles (EVs) are charged conductively where the vehicle charging port is connected to the supply by a wire. The plug-in charging system thus has the limitation of only being at a dedicated charging spot. Wireless power transfer (WPT) systems offer a convenient alternative to plugin charging, eliminating to need for manual intervention. The system can also be applicable for charging autonomous vehicles. A wireless transmitter pad can be installed underground and controlled from faraway stations.

An important part of high-power WPT systems is the design of the magnetic structures; the geometry, size, and materials contribute to the amount of coupling created between the transmitter and receiver. The amount of magnetic coupling also influences the amount of leakage magnetic flux around the charging system, which refers to the magnetic flux density that is exposed to anyone present near the charging system. The magnetic leakage flux is one of the most critical safety issues for WPT systems. For EVs, the International Commission on Non-Ionized Radiation Protection (ICNIRP) has limited the public exposure of the magnetic flux density to 27 μT at an 800 mm distance in all directions from the center of the pad [1].

Most WPT systems discussed in the literature consist of single-phase configurations [2], [3]. Although single-phase structures are ideal for low-power applications, they are not feasible for medium and high-power requirements. On the other hand, a three-phase system provides a faster and safer transfer of high power without exceeding the field emission and heat generation limits [4]. Moreover, these systems have the distinct advantages of reduced phase currents and a more uniform field distribution than single-phase systems [5]. All these factors have made three-phase WPT a potential candidate for transportation applications.

In recent years, there has been an increase in the research of three-phase WPT systems for various applications. Three-phase topologies for stationary charging have been conducted for low-power unmanned underwater vehicles and aerial drones [6], [7], [8], [9]. An alternative approach has been implemented to excite the three-phase pads with independent inverters and optimize their magnetic design and currents to achieve better coupling between the coils [10], [11]. In most cases, three-phase wireless charging systems have been studied for dynamic EV charging [12], [13], [14], [15], [16]. It is necessary to maintain a fixed battery voltage at the output of the receiver as the battery voltage is fixed on an EV [17]. Much research has been done to improve the power density, misalignment tolerance, and leakage emissions around the vehicle [18], [19], [20], [21], [22].

Three-phase stationary topologies have been studied for mostly unipolar and a few bipolar structures [23], [24], [25], [26], [27]. The existence of the interphase mutual inductance cannot be ignored in most cases and needs to be considered for determining the resonant frequency for multiphase systems.

One of the major challenges in a three-phase system coil design is the coil span, as it becomes smaller compared to a single-phase system, considering the coils need to fit in the same area. A solution to this problem is to fit multiphase coils into more than one layer [26], [28]. This strategy helps make the individual coil spans larger, which, in turn, helps achieve improved coupling. However, increased wire length can also yield higher losses, eventually reducing the system's efficiency.

This article proposes a novel three-phase double-layer overlapping winding (OW) based WPT system to overcome this constraint. The topology is presented in [28] with initial finite element analysis (FEA) results. The coils in the proposed system

Manuscript received 27 December 2022; revised 14 April 2023 and 24 June 2023; accepted 7 August 2023. Date of publication 28 August 2023; date of current version 23 October 2023. Recommended for publication by Associate Editor L. Wang. *(Corresponding author: Yilmaz Sozer.)*

The authors are with the Department of Electrical and Computer Engineering, University of Akron, Akron, OH 44325 USA (e-mail: src107@uakron.edu; mt106@uakron.edu; mh248@uakron.edu; ys@uakron.edu).

Color versions of one or more figures in this article are available at https://doi.org/10.1109/TPEL.2023.3309496.

Digital Object Identifier 10.1109/TPEL.2023.3309496

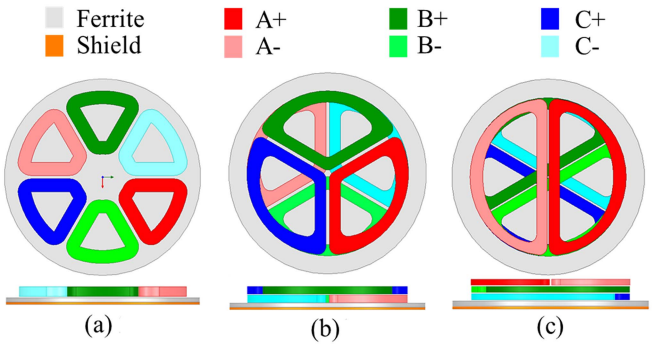

Fig. 1. Three-phase WPT topologies. (a) Single layer (SLNW) with coil span of 60°. (b) Double layer (DLOW) with coil span of 120°. (c) Triple layer (TLOW) with coil span of 180°.

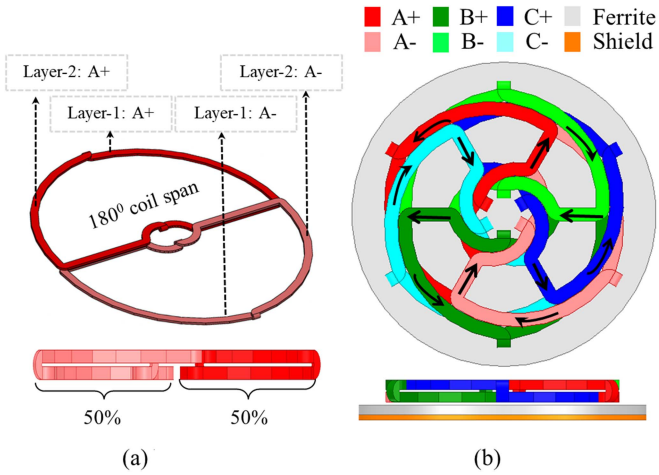

Fig. 2. Per-phase coil structure of the proposed overlapping winding, with 180° coil span. (a) Per-phase winding structure. (b) Overall winding structure.

have been designed to provide a satisfactory level of coupling with a shorter coil length. In addition, optimization has been carried out to maximize efficiency while maintaining the SAE J2954 standard [29]. A single-layer nonoverlapping winding (NW)–based three-phase WPT system has also been developed to certify the effectiveness of the proposed overlapping design. The optimized versions of both models have been compared in electromagnetic simulations. Moreover, a prototype of DL-OW based WPT system has been developed and tested.

The article starts with the winding structure development of the proposed WPT system and coil loss compared with other WPT structures in Section II. Section III describes the structure of the inductance matrices and the optimization method to finalize the dimensions of the proposed three-phase WPT system. A simulation-based performance comparison between the proposed and conventional WPT systems has been carried out in Section IV. The experimental results are demonstrated in Section V. Finally, Section VI concludes this article.

The current study includes several important contributions. Prototype development and experimental results of the proposed WPT system have been added. A comprehensive description of other three-phase WPT coil structures has been added along with the analysis of the inductance matrix. Moreover, steady-state thermal analysis has been included in the study to check the Tx and Rx coil temperature distribution. Finally, a misalignment study of the proposed WPT system has also been done.

II. Winding Structure Development and Comparative Loss Analysis of a Three-Phase WPT System

Single-layer NW (SLNW) with a coil span of 60°, double-layer OW (DLOW) with a coil span of 120°, and triple-layer OW (TLOW) with a coil span of 180° are the options discussed for three-phase WPT topologies [4], as shown in Fig. 1. All windings are on the same layer for the SLNW structure, as shown in Fig. 1(a), resulting in a same self-inductance for the individual windings and the same mutual inductances for the winding pairs; therefore, producing a balanced inductance matrix. This coil structure is easier to manufacture but suffers lower coupling between the transmitter and receiver. Although the amount of copper is less, a higher amount of current is required to flow to achieve the desired amount of power transfer due to lower coupling. As a result, the copper loss increases, lowering system efficiency.

In a double-layer structure, as shown in Fig. 1(b), layer-1 consists of all the negative coils (A-, B-, C-) and layer-2 consists of all the positive coils (A+, B+, C+), and therefore, winding on layer 1 and layer 2 has two different sets of self and mutual inductances. However, windings with different polarities of the same phase can be connected in series to obtain an overall balanced inductance for a double-layer structure with a coil span of 120°. This coil structure offers higher coupling between the transmitter and receiver. The triple-layer structure with a coil span of 180° can generate the highest coupling even more than other structures. However, for the 180° coil span, each layer contains a unique phase, and they are not equidistant from the ferrite layer, which creates a natural unbalance of self and mutual inductances.

A. Proposed Coil Structure of Three-Phase Windings

A novel two-layer structure with a coil span of 180° is proposed in this study to maximize the coupling with a balanced self and mutual inductance matrix. In this proposed three-phase WPT, each phase contains two coils. Each phase coil has an overlapping portion going linearly through the center. The half-circle arc for each bipolar structure has half of it on the top layer and half at the bottom as shown in Fig. 2.

The overall coil structure is circular shaped, overlapping the bipolar structures for the phases every 60° toward the center. Since half portion for positive coils (A+, B+, C+) and negative coils (A-, B-, C-) are in the top layer and the other half is in the bottom layer, and the positive and negative coils are connected in series, every phase is symmetric to ferrite layer. It produces a balanced self and mutual inductance matrix. Moreover, the direction of the current flow in the winding has been set in such a way that the flux generated in the overlapping coils of a phase adds up. This phenomenon results in higher coupling between the transmitter (Tx) and receiver (Rx). The direction of

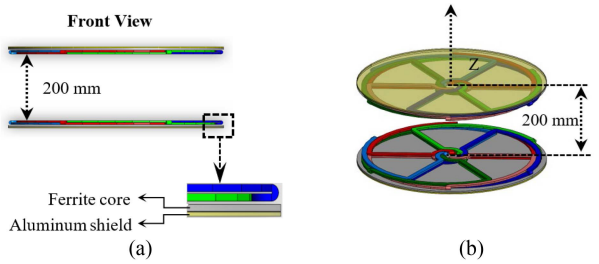

Fig. 3. (a) Front view of the proposed three-phase WPT system with ferrite core and aluminum shield. (b) Isometric view of the WPT system.

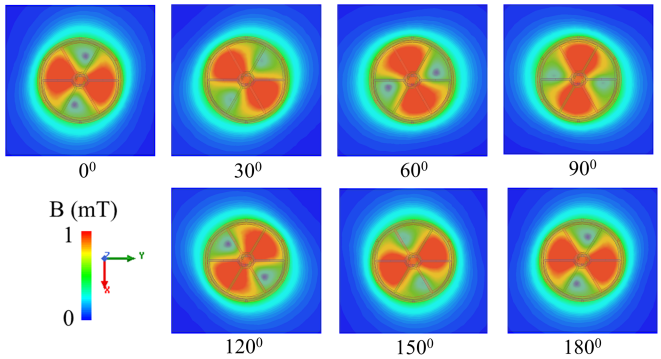

Fig. 4. Magnetic flux density through the center of the proposed WPT system along the *XY*-axis.

current flow in the proposed three-phase WPT system is shown in Fig. 2(b).

The dimensions of the WPT system can vary based on application requirements. In [30], the 7.7-kW system used a coil dimension of 600 mm × 800 mm with a 200-mm gap. The efficiency comparison of a 7.7-kW WPT system has been done with Tx and Rx coil dimensions of 470 mm × 95 mm and 470 mm × 365 mm, respectively in [31]. In [32], a 7.7-kW WPT system designed for EVs uses a rectangular coil with Tx and Rx dimensions of 364 mm × 364 mm and 329 mm × 329 mm, respectively. However, the dimension of the proposed coil will be determined based on an optimization.

The three-phase WPT system with Tx and Rx has been shown in Fig. 3. The windings are supported by a ferrite layer underneath and above the Tx and Rx coils, respectively. Each of the coils is equidistant from the ferrite layers, and thus when there is an alternating current flowing through them, the flux pattern will be uniform and symmetrical. The Tx and Rx pads were kept at a separation of 200 mm. The core layers of the Tx and Rx coils keep the magnetic flux concentrated between the Tx and Rx pads at the resonant frequency. The absence of core layers would have resulted in higher leakage flux and thus reduced mutual inductance. A picture of the rotating magnetic field can be seen along the *XY* plane going through the middle of the pads, as shown in Fig. 4. The rotating magnetic flux lines from the FEA-based simulations are seen to be rotating in a clockwise direction for the ABC sequence with the phase change.

In a three-phase overlapping wireless charging system, when ac current is passed through each coil, it creates its own magnetic

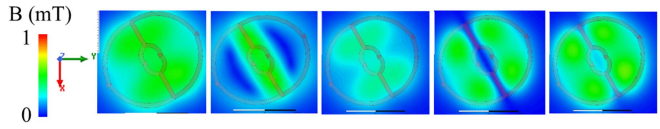

Fig. 5. Magnetic flux density through the center along the *XY*-axis with individual phase excitation (phase A).

field. The rotating magnetic field is created here by the phase difference between the ac currents flowing through each coil (120°), as shown in Fig. 4. Due to the spatial displacement of the windings, the magnetic field created by each phase is also displaced by 120° from each other. If the phases were excited individually, as shown in Fig. 5, where only phase A is excited, the magnitude gradient of the flux density is lower than when the excitation is three-phase.

B. Comparison of Coil Losses Between the Proposed and SLNW Three-Phase Topologies

The winding function of both SLNW and the proposed WPT system has been developed to start the analysis. Both the windings have the same inner and outer diameter, and the same air gap separates the Tx and Rx coils. The winding function can be considered as the MMF distribution for a unit winding current [33]. The MMF is expressed as

$$\tau(\theta) = n(\theta)\, i \tag{1}$$

where $n(\theta)$ is the turns function and $<n>$ is the average of the turns function over an interval. The winding function $N(\theta)$ can be expressed as

$$N(\theta) = n(\theta) - \langle n \rangle . \tag{2}$$

The turns function $n(\theta)$ depends on the reference position selected for the angle θ. The reference location for θ also affects the winding function $N(\theta)$ by introducing an arbitrary phase shift in the function. For a comparative analysis between two winding configurations, it is useful to define θ such that $N(\theta)$ will be unique for a given winding distribution. Due to the phases being 120° apart, the turns function of the two topologies can be represented by using the following equation:

$$n(\theta) = n_{ca}\ \cos\theta + n_{cb}\cos(\theta - 120) + n_{cc}\cos(\theta - 240) \tag{3}$$

where n_{ca}, n_{cb}, and n_{cc} are the winding pattern instantaneous values of the three phases of the coils. The value of $<n>$ in (2) turns out to be zero for both topologies. Fig. 6 represents the winding function for both topologies with a 0° reference angle.

If the number of turns is equal, then (3) can be represented as:

$$n(\theta) = N_s\cos\theta + N_s\cos(\theta - 120) + N_s\cos(\theta - 240) \tag{4}$$

where $n_{ca} = n_{cb} = n_{cc} = N_s$. A balanced three-phase current excitation can be written as

$$\begin{aligned} i_a(t) &= I_s\cos(2\pi f t) \\ i_b(t) &= I_s\cos(2\pi f t - 120^\circ) \\ i_c(t) &= I_s\cos(2\pi f t - 240^\circ) \end{aligned} \tag{5}$$

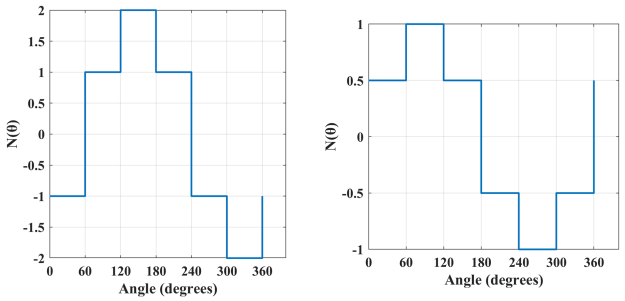

Fig. 6. Winding function for a reference angle of 0° of (a) proposed coil structure and (b) single-layer SLNW-based coil.

where I_s is the peak value of the current and f is the frequency of the excitation. So, the resultant magnetomotive force (MMF) can be expressed as

$$\begin{aligned} F(\theta,t) &= F_a\ (\theta,t) + F_b(\theta,t) + F_c(\theta,t) \\ &= N_s I_s[\cos\theta\cos(2\pi ft) \\ &\quad + \cos(\theta-120^\circ)\times\cos(2\pi ft-120^\circ) \\ &\quad + \cos(\theta-240^\circ)\times\cos(2\pi ft-240^\circ)] \\ &= \frac{3}{2}N_s I_s\cos(\theta-2\pi ft). \end{aligned} \tag{6}$$

So, the resultant MMF in the proposed three-phase WPT system will be rotating in nature and the direction will be radial.

The winding function can be considered as the MMF distribution for a unit winding current. If both winding topologies are to be operated under the same dc link voltage or the same MMF ($V_{\rm pr}$ and $V_{\rm SLNW}$ for the proposed and SLNW topologies, respectively) and the rate of change of flux is approximated identical for both topologies, the SLNW-based topology needs to have twice the number of turns compared to the proposed DLOW design based on the following equation:

$$\frac{V_{\rm pr}}{V_{\rm SLNW}} = \frac{2N_{\rm pr}}{N_{\rm SLNW}} \tag{7}$$

where $N_{\rm pr}$ and $N_{\rm SLNW}$ are the number of turns in the coil for the proposed and SLNW topology, respectively.

If the total coil loss of the proposed design is $P_{\rm loss(coil\text{-}pr)}$ with $N_{\rm OW}$ turns and $P_{\rm loss(coil\text{-}SLNW)}$ for the SLNW-based design with $N_{\rm SLNW}$ turns, the relation between the coil losses can be found as

$$\frac{P_{\rm loss(coil-pr)}}{P_{\rm loss(coil-SLNW)}} = \frac{R_{\rm pr}\left(I^2_{tx(pr)} + I^2_{rx(\rm pr)}\right)}{R_{\rm SLNW}\left(I^2_{tx(SLNW)} + I^2_{rx(\rm SLNW)}\right)} \tag{8}$$

where $R_{\rm pr}$ and $R_{\rm SLNW}$ are the wire resistances for the proposed and SLNW, respectively. To reduce the skin effect, Litz wires are used for high-frequency WPT systems, where each thin wire is individually insulated and stranded into a thicker conductor. Considering the same current through the coils, the equation reduces to the ratio between the coil resistances. Based on the relationship developed in (7), the relation between the number of turns required to generate the same amount of MMF can be shown as

$$N_{\rm pr} \approx 0.5 N_{\rm SLNW}. \tag{9}$$

If the coils are said to have the same outer diameter, the approximate length of the coils can be found. If the radius of the coil structure is r, then the coil length per turn in each phase for the proposed DLOW and SLNW-based designs based on geometrical approximation can be written as

$$l_{\rm pr} = (\pi r + 2r)\times 2 = r(2\pi+4) \tag{10}$$

$$l_{\rm SLNW} = \left(\frac{\pi r}{3} + 2r\right)\times 2 = r\left(\frac{2\pi}{3}+4\right) \tag{11}$$

$$\frac{l_{\rm pr}}{l_{\rm SLNW}} = 1.687. \tag{12}$$

Considering the same volume for the proposed and SLNW topology, the relation between the radii of the cross-sectional areas can be expressed as

$$\frac{r^2_{\rm pr}}{r^2_{\rm SLNW}} = \frac{l_{\rm SLNW}N_{\rm SLNW}}{l_{\rm pr}N_{\rm pr}} \tag{13}$$

where the coil cross-sectional areas are $A_{\rm pr}$ and $A_{\rm SLNW}$ and the radii of the cross sections are $r_{\rm pr}$ and $r_{\rm SLNW}$. The relation between the cross sections can thereby be found as

$$\frac{A_{\rm pr}}{A_{\rm SLNW}} = \frac{\pi r^2_{\rm pr}}{\pi r^2_{\rm SLNW}} = 1.185. \tag{14}$$

Using (6)–(10), the relation between the coil resistances and coil losses can be found as

$$\frac{P_{\rm loss(coil-pr)}}{P_{\rm loss(coil-SLNW)}} \approx \frac{R_{\rm pr}}{R_{\rm SLNW}} = \frac{\rho l_{\rm pr}N_{\rm pr}}{A_{\rm pr}}\,\frac{A_{\rm SLNW}}{\rho l_{\rm SLNW}N_{\rm SLNW}} = 0.712. \tag{15}$$

So, the proposed DLOW yields around 28.8% less coil loss compared to the NW with the same dimension and currents.

III. Inductance Matrix and Compensation Network

A. Inductance Matrix of the Three-Phase WPT System

As described earlier, the proposed WPT system utilizes three-phase OW windings on both the transmitter and receiver sides. The presence of a higher number of coils makes the formation of the inductance matrix more critical for a three-phase WPT system. The three-phase wireless charging system is represented with equivalent inductance parameters as shown in Fig. 7. The coils in the Tx and Rx coils are labeled as *L_t* and *L_r* with subscripts *a,b,c* representing the three phases. The inductances *Mt* and *Mr* with subscripts *a*, *b*, and *c* represent mutual inductances between Tx coils or Rx coils, whereas the terms *M_tr* and M_{txry} represent the mutual inductances between Tx and Rx coils. *M_tr* represents the mutual inductance between coils of the same phase and M_{txry} between the adjacent ones.

The three-phase WPT system consists of several mutual inductances as there are multiple coils in the system, and each will have a mutual flux linkage due to being in proximity of the other. The inductance matrix for the three-phase WPT system

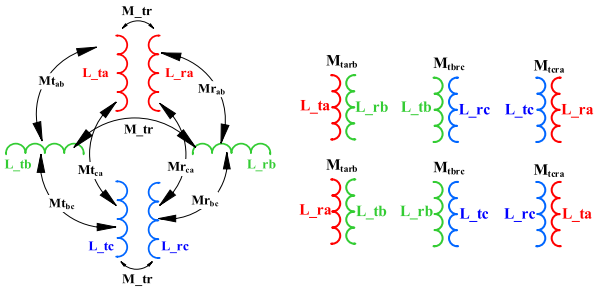

Fig. 7. Coils and their corresponding cross-coupling inductances of a three-phase magnetically coupled system.

can be shown as where V_a, V_b, and V_c are the phase voltages for phases a, b, and c, respectively. If the coils on each phase are identical, the matrix in (16) shown at the bottom of this page, will be a symmetric matrix. If the Tx and Rx coils are identical, the self-inductance and mutual inductances can be simplified into common terms. The 6×6 matrix is simplified with four distinct inductance values. The matrix becomes a symmetric matrix as shown in the following equation:

$$\begin{bmatrix} L & -M & -M & M_{tr} & -M_{txry} & -M_{txry} \\ -M & L & -M & -M_{txry} & M_{tr} & -M_{txry} \\ -M & -M & L & -M_{txry} & -M_{txry} & M_{tr} \\ -M_{tr} & -M_{txry} & -M_{txry} & L & -M & -M \\ -M_{txry} & -M_{tr} & -M_{txry} & -M & L & -M \\ -M_{txry} & -M_{txry} & -M_{tr} & -M & -M & L \end{bmatrix} \tag{17}$$

where L represents the coil self-inductances, M is the maximum mutual inductance between phases for either the Tx or the Rx coils, M_{tr} is the mutual inductance between the same set of Tx and Rx coil pairs, and M_{txry} is the mutual inductance between the different Tx and Rx coil pairs. In case of any parameter (e.g., coil turns, coil span, coil inner, and outer diameter) inconsistencies in any phase, the inductance matrix will be asymmetric and the self-inductance values will be different. This will reduce the coupling coefficient, efficiency, and power transfer capability of the three-phase WPT system. Furthermore, phase currents will also be imbalanced because of this. These unbalanced currents will also increase the size of the power converter and the thermal stress will be different in each phase. When the primary and secondary voltages and currents are balanced, the three-phase system can be transformed into an equivalent single-phase WPT system [5], [23]. The equivalent coil inductances can be expressed as

$$L' = L + M. \tag{18}$$

B. Compensation Networks

Due to the significantly large air gap between the Tx and Rx coils, the coupling coefficient between these coils is relatively lower. Thus, resonant tuning is needed with capacitive compensation to achieve a power factor correction and, thus, improve system efficiency.

The most common forms of compensation topology for single-phase WPT systems are series–series, series–parallel, parallel–series, parallel–parallel, LCC-S, and LCC-LCC compensation. Each topology has its pros and cons and is a separate scope of research. The *LCC* configuration is the most frequently used multicomponent compensation topology for a WPT system and is more suitable for misaligned cases, especially for dynamic wireless charging systems, where the coupling coefficient is constantly changing. As the coil currents are independent of the coupling for the *LCC* compensated topology [34], it is more suitable for dynamic charging and misaligned coils.

For polyphase systems, the compensation network can be either Y or Δ connected or a combination of both [34], so four different combinations can be possible (Y-Y, Y-Δ, Δ-Y, Δ-Δ). Compensation networks like *LCC* have not been implemented as they will create a more complex system to achieve perfect resonance in an already complex polyphase network involving multiple cross-coupling terms. For Y-Y and Δ- Δ connected systems in a perfectly balanced condition, the compensation capacitor values can be determined using the following equation:

$$C' = \frac{1}{\omega^2 L'}. \tag{19}$$

Similarly, for Δ-Y and Y-Δ configurations, the compensation capacitor values can be determined as [10]

$$C' = \frac{1}{3\omega^2 L'} \tag{20}$$

$$C' = \frac{3}{\omega^2 L'}. \tag{21}$$

IV. Comparison of Coil Topologies Under the Same Operating Conditions

This section primarily provides the efficiency comparison between SLNW and the proposed winding structure. Moreover, the proposed WPT structure's inductance matrices are being compared with the state-of-the-art TLOW winding structure. At

$$\begin{bmatrix} V_a \\ V_b \\ V_c \\ 0 \\ 0 \\ 0 \end{bmatrix} = \begin{bmatrix} L_{ta} & -Mt_{ab} & -Mt_{ca} & M_{tr} & -M_{tarb} & -M_{tarc} \\ -Mt_{ab} & L_{tb} & -Mt_{bc} & -M_{tarb} & M_{tr} & -M_{tbrc} \\ -Mt_{ca} & -Mt_{bc} & L_{tc} & -M_{tarc} & -M_{tbrc} & M_{tr} \\ M_{tr} & -M_{tarb} & -M_{tarc} & L_{ra} & -Mr_{ab} & -Mr_{ca} \\ -M_{tarb} & M_{tr} & -M_{tbrc} & -Mr_{ab} & L_{rb} & -Mr_{bc} \\ -M_{tarc} & -M_{tbrc} & M_{tr} & -Mr_{ca} & -Mr_{bc} & L_{rc} \end{bmatrix} \begin{bmatrix} I_{ta} \\ I_{tb} \\ I_{tc} \\ I_{ra} \\ I_{rb} \\ I_{rc} \end{bmatrix} \tag{16}$$

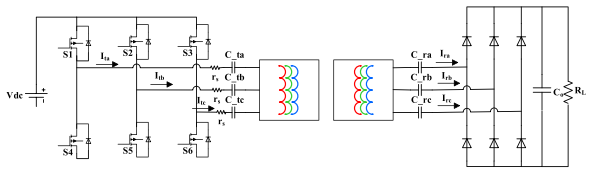

Fig. 8. Circuit prototype for testing the three-phase WPT system with series–series compensation network.

first, a Simulink-based three-phase WPT system was developed with a series–series compensation. The inductance matrix calculated from 3-D FEA simulation has been provided to represent the three-phase winding in this system. Based on the developed WPT system, an optimization method has been implemented to maximize the overall efficiency of conventional SLNW and the proposed three-phase WPT structure.

A. Optimization of the OW-Based Designs

To find the optimized conventional SLNW and proposed OW-based three-phase wireless charger pad design, an optimization scheme was developed. An SAE-standardized single-phase wireless charger system described in [35] has been chosen as the benchmark model for this purpose. The Tx and Rx coil shape is circular for the single-phase benchmark model. The Tx and Rx coil dimensions are 650 mm × 500 m and 380 mm × 380 mm, respectively. Both Tx and Rx coils used Litz wire with 1260 strands of AWG 38 insulated wires. The equivalent external diameter of the coil is 5 mm. The bulk coil outer diameter, height, and thickness were changed for each case to obtain the initial set of designs. Based on the design constraints, the second set of designs was filtered, and the final design was chosen with the highest system efficiency. For each design set, the FEA simulations were performed. The simulation and test platform included a dc supply, a three-phase inverter, the compensation networks, a three-phase rectifier, and a resistive load, as shown in Fig. 8.

The detailed flowchart to achieve the optimized design is shown in Fig. 9.

The inverter's output terminals were connected to the Tx coils operating at 180° conduction mode, where the line-to-line (L-L) voltages and phase currents are separated by 120°. The Litz wire ac and dc resistances were used to calculate coil losses based on standard resistance methods. The coil currents from the simulation model were used to calculate the FEA model's core and shield losses. The core material chosen was 3C95 material by Ferroxcube. For the specific type of ferrite, the Steinmetz parameters were found from the core loss versus frequency model for power ferrite. The inverter switching and conduction losses were calculated for the SiC modules used on the experimental prototype. The rectifier diode losses were calculated for the prototype diode module based on ultrafast Schottky diodes. The final parameters of the proposed system are shown in Table I.

B. Simulation Results

The series compensation capacitors cancel the leakage flux and higher-order harmonics. As a result, the currents only have

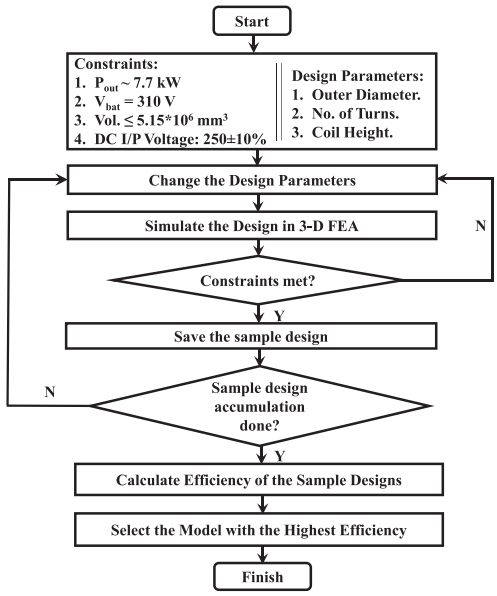

Fig. 9. Brute-force optimization flowchart of three-phase WPT system.

TABLE I
FINAL DESIGN PARAMETERS OF THE PROPOSED SYSTEM

Parameter	OW-based design
Inner diameter (mm)	64
Outer diameter (mm)	572
Litz wire	1600/38
Number of turns	3
Compensating capacitor value (nF)	42.4
Input dc link voltage	261.5
Overall coil volume of both pads (mm^3)	1.3×10^6
Overall core volume (mm^3)	2.43×10^6

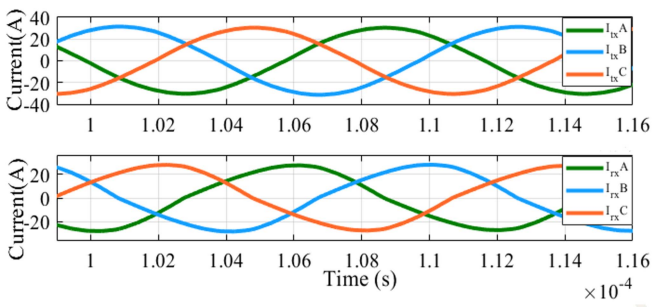

Fig. 10. Tx and Rx currents of the three-phase OW-based WPT system for 7.7 kW output power with $V_{\text{battery}} = 310$ V.

fundamental Tx and Rx coil currents of the final three-phase DLOW-based design operating at 85 kHz, as shown in Fig. 10 .

To measure the magnetic field emissions of the WPT system, an observation circle with a radius of 800 mm from the center of the Tx coils was created, as shown in Fig. 11.

According to ICNIRP guidelines, the rms value of the leakage flux at an 800 mm distance from the center of the pads should be less than 27 μTRMS. According to the figure, the leakage flux is below the threshold for any phase. The magnetic field

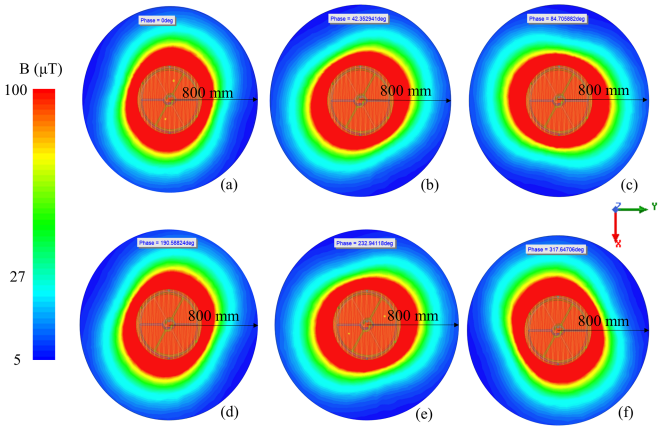

Fig. 11. Magnetic field density at different phases, i.e., (a) 0°, (b) 42°, (c) 84°, (d) 190°, (e) 232°, and (f) 317°, around an 800-mm circle around the center of the Tx pads.

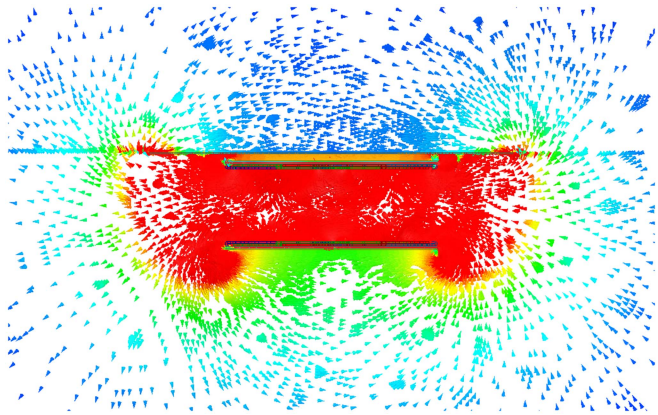

Fig. 12. Magnetic field vector lines along the vertical *YZ*-axis.

intensity keeps changing with an elliptical shape, but it does not exceed the limit provided by ICNIRP. An additional aluminum shield was placed in addition to the aluminum shield attached to the Rx coil to further reduce emissions inside the vehicle for passenger protection. Fig. 12 shows the direction of the magnetic flux vectors with the phase change. The magnetic field lines were suppressed with the addition of the shield layer above the Rx pad. The total coil current is passing through each of the compensation capacitors per phase so it is evident that these voltages across the capacitors will be high as the impedance of the capacitors will be high due to the high switching frequency.

To check Tx and Rx coil temperature, steady-state thermal analysis has been done for the proposed WPT system. The loss per volume values for coil, ferrite, and aluminum shield have been provided as inputs in the analysis. Furthermore, the convection heat transfer coefficient of 1 W/m^{2}K has been considered for the outer surface. The coil temperature distribution from the thermal analysis has been shown in Fig. 13.

The maximum temperature in Tx and Rx coils is 53.6 °C and 68.72 °C, respectively. Although steady-state thermal analysis shows a temperature gradient in coil geometries, the gap between the maximum and minimum temperature is low.

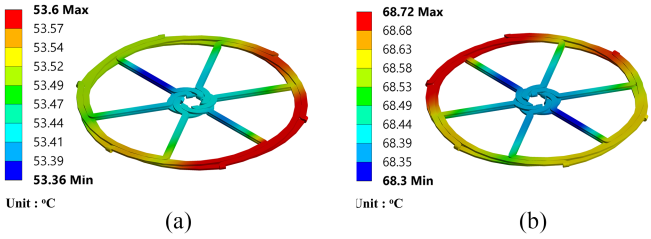

Fig. 13. Temperature distribution of (a) Tx coil and (b) Rx coil.

TABLE II
OPTIMIZED DESIGN PARAMETERS OF SLNW AND PROPOSED WPT SYSTEMS

Parameter	SLNW Design	Proposed Design
Inner diameter (mm)	66	64
Outer diameter (mm)	572	572
Litz wire	1250/38	1600/38
Number of turns	7	3
Compensating capacitor(nF)	31.4	42.4
Input dc link voltage	261	261.5
Current (A_{rms}): Tx	25	23.08
Current (A_{rms}): Rx	19.26	19.46
$R_{ac}+R_{dc}$ (mΩ) per ph.	39.96	30.58
Coil losses (W)	130.26	83.62
Core loss (W)	52.67	49.53
Shield loss (W)	3.2	2.94
Power electronic loss (W)	268.17	253.6
B_{max} at observation (μT)	10.8	10.9

For comparative analysis between the proposed DLOW and conventional SLNW coils, the overall coil weight was kept the same for both designs. Also, the ferrite core thickness and shield thickness were kept the same. As a result, the power densities for both the proposed and SLNW-based systems are equal. The parameters found from the final OW and NW-based design simulation are given in Table II.

The simulation results show that the ratio between the coil losses for the proposed and SLNW designs is 0.65, which is very close to the predictions made in (12). The overall gravimetric power density of the proposed system turned out to be 6.0% higher than the benchmark single-phase WPT model and 2.90% higher in terms of system efficiency. Compared to the three-phase NW system, the proposed OW offers 0.9% more efficiency maintaining similar volumetric and gravimetric power density. The optimized design and simulated efficiencies use the same power electronic converter parameters for all the cases for a fair comparison. Moreover, a slightly higher switching frequency has been used to operate above resonance to maintain a lagging current, which helps to discharge the output capacitors of the MOSFET during the dead time and bring the voltage to zero level before the MOSFET is turned ON. This zero voltage switching (ZVS) has been considered for all the cases to eliminate the turn ON losses of the converter. The detailed performance analysis for the three systems is summarized in Table III.

The proposed three-phase DLOW design has 2.9% higher efficiency than that of the benchmark model. A three three-phase WPT system generates smaller per-phase current amplitudes for the system, which helps to reduce the copper loss. The rms currents in Tx and Rx coil of the single-phase benchmark model are 81.6 A and 21.3 A, respectively. On the other hand,

TABLE III
PERFORMANCE COMPARISON BETWEEN THE BENCHMARK SLNW AND PROPOSED DLOW WIRELESS CHARGING SYSTEMS

Model	Bench mark	3-phase SLNW	3-phase proposed
System efficiency (%)	92.00	94.0	94.9
Coupling between Tx and Rx	0.148	0.111	0.1409
Total volume (m3)	0.0515	0.050742	0.05074
Coil weight (kg)	10.73	9.16	9.159
Total core weight (kg)	12.22	11.79	11.79
Total shield weight (kg)	3.88	4.39	4.39
Volumetric power density (kW/m3)	1504	1515.7	1515.8
Gravimetric power density (kW/kg)	0.287	0.304	0.304

TABLE IV
SIMULATED INDUCTANCE MATRIX (IN μH) BETWEEN THE COILS OF THE PROPOSED WPT SYSTEM

	Atx	Btx	Ctx	Arx	Brx	Crx
Atx	**31.08**	6.99	6.97	3.57	1.69	1.68
Btx	7.04	**31.05**	7.02	1.71	3.60	1.69
Ctx	7.04	7.02	**31.06**	1.70	1.71	3.59
Arx	3.58	1.68	1.68	**31.06**	7.00	6.98
Brx	1.70	3.58	1.69	6.97	**31.05**	6.99
Crx	1.70	1.71	3.59	7.02	7.03	**31.08**

The bold entities indicate the self-inductances.

TABLE V
SIMULATED INDUCTANCE MATRIX (IN μH) BETWEEN THE COILS OF THE TLOW WPT SYSTEM

	Atx	Btx	Ctx	Arx	Brx	Crx
Atx	**27.71**	19.33	18.14	1.97	1.90	1.87
Btx	19.33	**30.40**	21.90	1.90	1.87	1.82
Ctx	18.14	21.90	**35.92**	1.87	1.82	1.81
Arx	1.97	1.90	1.87	**27.75**	19.37	18.19
Brx	1.90	1.87	1.82	19.37	**30.45**	21.95
Crx	1.87	1.82	1.81	18.19	21.95	**35.98**

The bold entities indicate the self-inductances.

TABLE VI
SIMULATED INDUCTANCE MATRIX (IN μH) BETWEEN THE COILS OF THE DLOW WPT SYSTEM WITH 120° COIL SPAN

	Atx	Btx	Ctx	Arx	Brx	Crx
Atx	**27.05**	8.17	8.17	1.52	0.75	0.75
Btx	8.17	**27.04**	8.16	0.75	1.52	0.75
Ctx	8.17	8.16	**27.05**	0.75	0.75	1.52
Arx	1.52	0.75	0.75	**27.06**	8.17	8.16
Brx	0.75	1.52	0.75	8.17	**27.06**	8.17
Crx	0.75	0.75	1.52	8.16	8.17	**27.05**

The bold entities indicate the self-inductances.

in the proposed structure, the rms currents in Tx and Rx coil are 23.08 A and 19.46 A, respectively.

Tables IV and V show the simulated inductance matrices for the proposed DLOW and TLOW winding structures, respectively. Although the coil span of these two structures is the same, the proposed structure shows superior performance in balance inductance matrices. The same optimized parameters for the proposed system are used to calculate the inductance matrices for the TLOW WPT system.

Table VI shows the simulated inductance matrix of the DLOW WPT system with a 120° coil span. The number of turns and inductances have been calculated considering the same dc link operating voltage. The mutual inductance values between the transmitter and receiver of the same phase are lower in this configuration. As a result, the resulting coupling coefficient will be lower compared to the proposed structure. Although

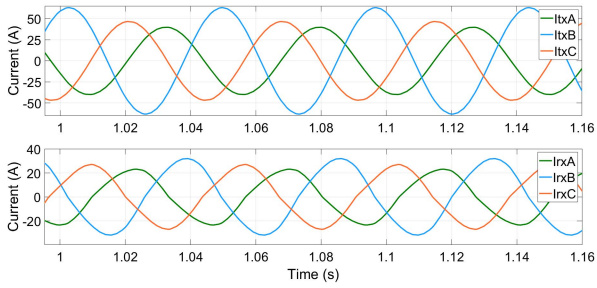

Fig. 14. Tx and Rx currents of the three-phase OW-based WPT system at maximum misaligned conditions along X (100 mm) and Y (75 mm) axes, for 7.7 kW output power and $V_{\mathrm{battery}} = 310$ V.

TABLE VII
LOSSES ON THE PROPOSED WPT SYSTEM FOR MAXIMUM LATERAL MISALIGNMENT ($\Delta X = 100$ MM, $\Delta Y = 75$ MM)

Parameter	Values
Current (A_{rms}): TxA, TxB, TxC	28.25, 47.02, 33.41
Current (A_{rms}): RxA, RxB, RxC	16.84, 21.21, 18.42
R_{ac}+R_{dc} (mΩ) per ph.	30.58
Coil losses (W)	126.15
Core loss (W)	60.56
Shield loss (W)	3.7
Power electronic loss (W)	361
Overall system efficiency (%)	92.82

this structure provides lower copper loss due to the absence of end winding, it has the disadvantage of a lower coupling coefficient than that of the 180° span. Considering this, DLOW with a 180° span can be considered the optimal solution for high power transfer applications.

This study also examines the effect of coil misalignment for the proposed three-phase DLOW system. According to the SAE J2954 standard, the following two parameters are important to evaluate the performance of the WPT system during the misalignment: 1) the distance between the Tx coil and the lateral side of the vehicle and 2) the distance between the Tx coil and front (or back) side of the vehicle [29]. In this study, the performance of the proposed WPT system was checked for lateral misalignment at $\Delta x = 100$ mm and $\Delta y = 75$ mm. Fig. 14 shows Tx and Rx phase currents during the misalignment.

Table VII shows the output parameters of the WPT systems operating with the misalignment. All the loss components of the proposed WPT system increased during the misalignment. As a result, the efficiency of the WPT system drops from 94.9% to 92.82%.

V. EXPERIMENTAL PROTOTYPE DESIGN AND VALIDATION

A. Prototype System

The experimental prototype of the three-phase WPT system is shown in Fig. 15(a). It has the same outer diameter with two-layer overlapping coils as the proposed structure. The start and end terminals of each phase coil were from the same slot and each phase terminal was 120° apart from each other. The coils were supported by a Plexiglas sheet, followed by a layer of ferrite and an aluminum shield. Fig. 15(b) shows the three-phase SiC MOSFET-based inverter used for validation. It uses Cree's

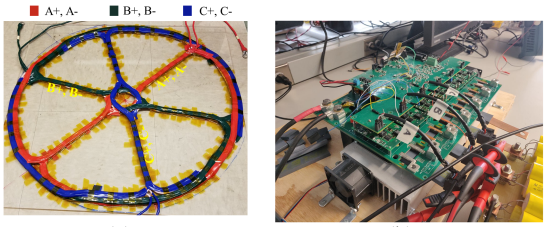

(a) (b)

Fig. 15. (a) Experimental coil setup showing the winding pattern at 120° phase apart. (b) SiC three-phase inverter used for experimental validation.

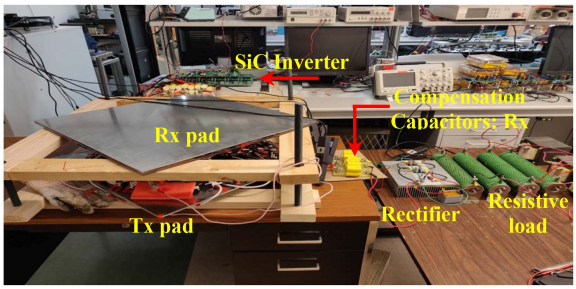

Fig. 16. Experimental setup at the perfect alignment between the coils.

TABLE VIII
MEASURED INDUCTANCE MATRIX (IN μH) BETWEEN THE COILS OF THE PROPOSED WPT SYSTEM USING LCR METER

	Atx	Btx	Ctx	Arx	Brx	Crx
Atx	**29.46**	5.345	4.7	1.895	0.925	0.62
Btx	5.345	**28.56**	4.6	0.835	2.04	0.685
Ctx	4.7	4.6	**28.46**	0.85	0.545	1.535
Arx	1.895	0.835	0.85	**30.07**	5.095	4.965
Brx	0.925	2.04	0.545	5.095	**29.56**	5.17
Crx	0.62	0.685	1.535	4.965	5.17	**29.23**

The bold entities indicate the self-inductances.

three SiC half-bridge modules (1200 V/325 A) and gate drivers (UCC21750) from Texas Instruments.

Fig. 16 shows the overall prototype system. For the uncontrolled rectifier, three ultrafast diode modules (VS-UFB280FA40) from Vishay were used for the three legs. The inverter consists of 340 μF dc capacitor bank at the input terminals with a common mode electromagnetic interference choke for the reduction of electromagnetic interference. A Texas Instrument TMS320F28377D DSP-based control board has been used to generate the three-phase open loop voltage pattern required to drive the proposed three-phase WPT system.

The self and mutual inductances of the proposed WPT system have been measured using an Agilent E4980A precision LCR meter. The measured inductance matrix of the proposed three-phase WPT system for the perfectly aligned condition is shown in Table VIII. The matrix is symmetric, as claimed in (14).

B. Experimental Results

The system was tested at 2.4 kW output power to validate the system's performance. Fig. 17 shows the Tx L-N voltages and line currents of the three phases and the Rx coil currents. To operate the inverter at ZVS, the WPT system was operated

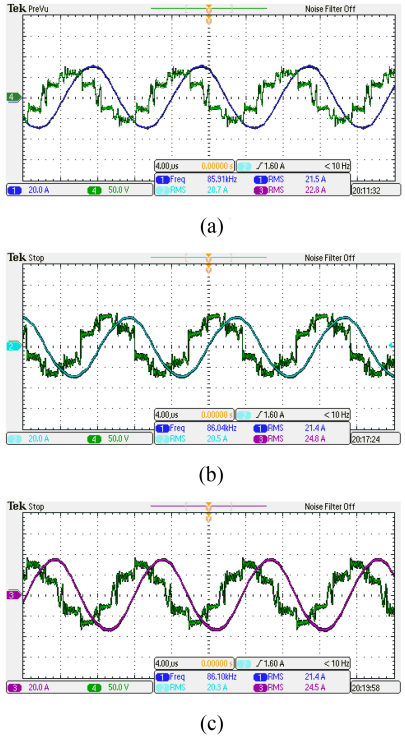

(a) (b) (c)

Fig. 17. Measured line currents with L-N voltages for Tx coil for the proposed three-phase WPT system operating at 86 kHz resonant frequency at perfect alignment with 2.4 kW output power. (a) Tx: $V_{\rm an}$ versus $I_{\rm a}$. (b) Tx: $V_{\rm bn}$ versus $I_{\rm b}$. (c) Tx: $V_{\rm cn}$ versus $I_{\rm c}$.

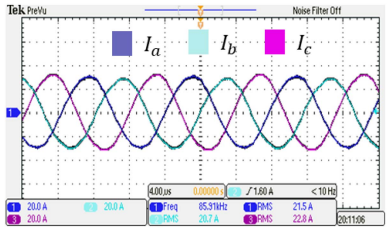

Fig. 18. Measured line currents (Tx side) of the proposed three-phase WPT system operating at 86 kHz resonant frequency at perfect alignment with 2.4 kW output power.

slightly higher than the resonant frequency, which minimizes the switching loss at the inverter.

The ripples on the line-neutral voltage waveforms in Fig. 17 are due to a high-frequency common-mode voltage showing up on the neutral point. The larger and unequal cable length for neutral point connections, as shown in Fig. 13, of the transmitter and receiver coil also caused this common mode voltage bouncing. A Yokogawa WT3000 power analyzer was used to measure the dc input power, dc output power, and dc–dc system efficiency.

The balanced coil structure of the proposed system generates balanced line currents, as shown in Fig. 18. Fig. 19 shows the magnetic field emissions at 800 mm distance from the center of the coils. The leakages were below the threshold limits (27 μTRMS) for the target output power.

The system was further tested up to 5 kW output power as shown in Fig. 20, but due to limitations of the resonant capacitor and diode current ratings, the system was scaled down to be

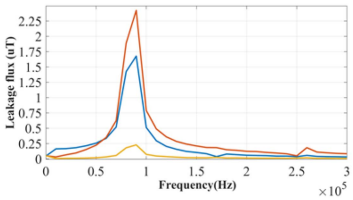

Fig. 19. Magnetic field emissions at perfectly aligned conditions with peaks along the three axes located near 86–88 kHz frequency, resulting in maximum leakage flux around 2.42 μT.

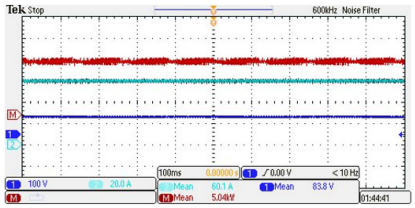

Fig. 20. Output voltage and power at perfectly aligned conditions of the proposed system operating at 37.7 kHz switching frequency with 5.04 kW output power across the load terminal.

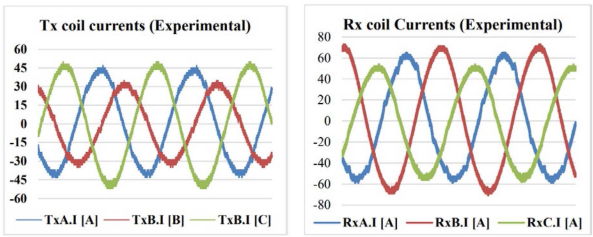

Fig. 21. Current waveforms of the three-phase WPT system working at 37.8 kHz resonant frequency for 5 kW output power showing (a) Tx currents and (b) Rx currents.

tested at 37–38 kHz frequency. Also, due to the lower operating frequency, the air gap between the Tx and Rx coils was lowered to 150 mm instead of 200 mm to achieve better coupling and less leakage for safer operation. The measured efficiency of the proposed WPT system is found to be 93.55%, which supports the claim of efficiency improvement compared to the benchmark system. Fig. 21 shows the Y-Y connected coil currents on the Tx and Rx coils from the simulation and experimental setup for 5 kW output power.

VI. Conclusion

A 7.7-kW three-phase WPT system based on OWs has been presented in this study for fast charging of EV powertrains. A comparative analysis for a single-layer and proposed double-layer winding-based three-phase system was shown with simulation results. The system efficiency of the proposed topology came out to be 94.93%, which was 2.93% higher than the benchmark model and 0.81% higher than the existing three-phase nonoverlapping topology. An identical experimental prototype was built using 800/38 Litz wires, and the balance inductance matrix claim has been experimentally validated. The proposed system has been tested at 86 kHz resonant frequency and 2.4 kW output power condition, and at 37 kHz resonant frequency with 5.04 kW output power, resulting in 93.55% system efficiency, proving the proposed WPT structure compared to the benchmark system.

The main advantages of the proposed three-phase DLOW system include scalability, flexibility, and high power transfer capability. The proposed system can be scaled up to meet high power (∼100 kW or above) requirements. In that case, the improvement in terms of efficiency, power density, and coil weight would be much higher than single-phase WPT systems. In addition, the proposed three-phase WPT system has the flexibility of changing winding configuration (coils per turn, end winding length, etc.) to adjust system requirements. Furthermore, the power converter of the three-phase WPT system requires less capacitance and rms current stress in the capacitor in the rectifier stage than the single-phase WPT. It increases converter power density and lifetime. As a result, the proposed structure provides a more efficient solution to transfer a high amount of power much faster than the conventional state-of-the-art options. However, the Litz wire bending on the proposed solution will increase the overall volume slightly. More advanced techniques, such PCB-based winding, could be a scope of future study to use the proposed scheme without impacting the volume due to bending.

The future works of the study include the development of 3-D printed fixtures to maintain the consistency of the proposed DLOW coils. Moreover, maintaining the concentricity of Tx and Rx coils to reduce the deviations in the inductance matrix is a priority. The current mechanical assembly is not suitable for conducting performance analysis during the misalignment. So, the development of a new mechanical assembly and experimental validation of the three-phase WPT system for misalignment has also been included in a future study.

References

[1] J. Lin et al., "ICNIRP guideline for limiting exposure to time-varying electric and magnetic fields (1 Hz-100 kHz)," *Health Phys.*, vol. 99, no. 6, pp. 818–836, 2010.

[2] D. Patil, M. K. McDonough, J. M. Miller, B. Fahimi, and P. T. Balsara, "Wireless power transfer for vehicular applications: Overview and challenges," *IEEE Trans. Transp. Electrific.*, vol. 4, no. 1, pp. 3–37, Mar. 2018.

[3] G. A. Covic and J. T. Boys, "Inductive power transfer," *Proc. IEEE*, vol. 101, no. 6, pp. 1276–1289, Jun. 2013.

[4] J. Pries, V. P. N. Galigekere, O. C. Onar, and G.-J. Su, "A 50-kW three-phase wireless power transfer system using bipolar windings and series resonant networks for rotating magnetic fields," *IEEE Trans. Power Electron.*, vol. 35, no. 5, pp. 4500–4517, May 2020.

[5] H. Matsumoto, Y. Neba, H. Iura, D. Tsutsumi, K. Ishizaka, and R. Itoh, "Trifoliate three-phase contactless power transformer in case of winding-alignment," *IEEE Trans. Ind. Electron.*, vol. 61, no. 1, pp. 53–62, Jan. 2014, doi: 10.1109/TIE.2013.2242421.

[6] T. Kan, R. Mai, P. P. Mercier, and C. C. Mi, "Design and analysis of a three-phase wireless charging system for lightweight autonomous underwater vehicles," *IEEE Trans. Power Electron.*, vol. 33, no. 8, pp. 6622–6632, Aug. 2018.

[7] T. Kan, Y. Zhang, Z. Yan, P. P. Mercier, and C. C. Mi, "A rotation resilient wireless charging system for lightweight autonomous underwater vehicles," *IEEE Trans. Veh. Technol.*, vol. 67, no. 8, pp. 6935–6942, Aug. 2018.

[8] C. Song et al., "Three-phase magnetic field design for low EMI and EMF automated resonant wireless power transfer charger for UAV," in *Proc. IEEE Wireless Power Transf. Conf.*, 2015, pp. 1–4.

[9] C. Song et al., "EMI reduction methods in wireless power transfer system for drone electrical charger using tightly coupled three-phase resonant magnetic field," *IEEE Trans. Ind. Electron.*, vol. 65, no. 9, pp. 6839–6849, Sep. 2018.

[10] S. Kim, G. A. Covic, and J. T. Boys, "Tripolar pad for inductive power transfer systems for EV charging," *IEEE Trans. Power Electron.*, vol. 32, no. 7, pp. 5045–5057, Jul. 2017.
[11] S. Kim, G. A. Covic, and J. T. Boys, "Comparison of tripolar and circular pads for IPT charging systems," *IEEE Trans. Power Electron.*, vol. 33, no. 7, pp. 6093–6103, Jul. 2018.
[12] G. A. Covic, J. T. Boys, M. L. G. Kissin, and H. G. Lu, "A three-phase inductive power transfer system for roadway-powered vehicles," *IEEE Trans. Ind. Electron.*, vol. 54, no. 6, pp. 3370–3378, Dec. 2007.
[13] D. J. Thrimawithana and U. K. Madawala, "A three-phase bi-directional IPT system for contactless charging of electric vehicles," in *Proc. IEEE Int. Symp. Ind. Electron.*, 2011, pp. 1957–1962.
[14] H. Li, Y. Liu, K. Zhou, Z. He, W. Li, and R. Mai, "Uniform power IPT system with three-phase transmitter and bipolar receiver for dynamic charging," *IEEE Trans. Power Electron.*, vol. 34, no. 3, pp. 2013–2017, Mar. 2019.
[15] H. Matsumoto, Y. Shibako, Y. Shiihara, R. Nagata, and Y. Neba, "Three-phase lines to single-phase coil planar contactless power transformer," *IEEE Trans. Ind. Electron.*, vol. 65, no. 4, pp. 2904–2914, Apr. 2018.
[16] J. Huh, W. Lee, G.-H. Cho, B. Lee, and C.-T. Rim, "Characterization of novel inductive power transfer systems for on-line electric vehicles," in *Proc. IEEE Appl. Power Electron. Conf. Expo.*, 2011, pp. 1975–1979.
[17] M. Khalilian and P. Guglielmi, "A dual-topology wireless power transfer system with constant current or constant voltage output for battery charging application," *Int. J. Eng. Res. Technol.*, vol. 12, no. 2, pp. 237–244, 2019.
[18] Z. Luo and X. Wei, "Analysis of square and circular planar spiral coils in wireless power transfer system for electric vehicles," *IEEE Trans. Ind. Electron.*, vol. 65, no. 1, pp. 331–341, Jan. 2018.
[19] S. Park, "Evaluation of electromagnetic exposure during 85 kHz wireless power transfer for electric vehicles," *IEEE Trans. Magn.*, vol. 54, no. 1, Jan. 2018, Art. no. 5100208.
[20] F. Y. Lin, G. A. Covic, and J. T. Boys, "Leakage flux control of mismatched IPT systems," *IEEE Trans. Transp. Electrific.*, vol. 3, no. 2, pp. 474–487, Jun. 2017.
[21] S. Y. Choi, B. W. Gu, S. W. Lee, W. Y. Lee, J. Huh, and C. T. Rim, "Generalized active EMF cancel methods for wireless electric vehicles," *IEEE Trans. Power Electron.*, vol. 29, no. 11, pp. 5770–5783, Nov. 2014.
[22] H. Kim et al., "Coil design and measurements of automotive magnetic resonant wireless charging system for high-efficiency and low magnetic field leakage," *IEEE Trans. Microw. Theory Techn.*, vol. 64, no. 2, pp. 383–400, Feb. 2016.
[23] H. Matsumoto, Y. Neba, K. Ishizaka, and R. Itoh, "Model for a three-phase contactless power transfer system," *IEEE Trans. Power Electron.*, vol. 26, no. 9, pp. 2676–2687, Sep. 2011.
[24] Y. Song, U. K. Madawala, T. Duleepa J, and A. P. Hu, "Cross coupling effects of poly-phase bi-directional inductive power transfer systems used for EV charging," in *Proc. IEEE Int. Future Energy Electron. Conf.*, 2015, pp. 1–7.
[25] Y. Song, U. K. Madawala, D. J. Thrimawithana, and A. P. Hu, "LCL and CL compensations for wireless three phase bi-directional EV charging systems," in *Proc. IEEE Southern Power Electron. Conf.*, 2016, pp. 1–6.
[26] K. Kusaka, R. Kusui, J. Itoh, D. Sato, S. Obayashi, and M. Ishida, "A 22 kW-85 kHz three-phase wireless power transfer system with 12 coils," in *Proc. IEEE Energy Convers. Congr. Expo.*, 2019, pp. 3340–3347.
[27] H. Matsumoto, R. Nakashima, Y. Neba, and H. Asahara, "Proposal and verification of two-layer three-phase contactless power transformer," *IEEJ Trans. Ind. Appl.*, vol. 135, no. 5, pp. 539–547, 2015.
[28] S. Chowdhury, M. T. B. Tarek, and Y. Sozer, "Design of a 7.7 kW three-phase wireless charging system for light duty vehicles based on overlapping windings," in *Proc. IEEE Energy Convers. Congr. Expo.*, 2020, pp. 5169–5176.
[29] *Wireless Power Transfer for Light-Duty Plug-In/Electric Vehicles and Alignment Methodology*, J2954_202010, 2017.
[30] W. Li, H. Zhao, J. Deng, S. Li, and C. C. Mi, "Comparison study on SS and double-sided LCC compensation topologies for EV/PHEV wireless chargers," *IEEE Trans. Veh. Technol.*, vol. 65, no. 6, pp. 4429–4439, Jun. 2016, doi: 10.1109/TVT.2015.2479938.
[31] D. Vincent, S. Chakraborty, P. S. Huynh, and S. S. Williamson, "Efficiency analysis of a 7.7 kW inductive wireless power transfer system with parallel displacement," in *Proc. IEEE Int. Conf. Ind. Electron. Sustain. Energy Syst.*, 2018, pp. 409–414, doi: 10.1109/IESES.2018.8349911.
[32] Y. Yang, M. El Baghdadi, Y. Lan, Y. Benomar, J. Van Mierlo, and O. Hegazy, "Design methodology, modeling, and comparative study of wireless power transfer systems for electric vehicles," *Energies*, vol. 11, no. 7, Jul. 2018, Art. no. 1716, doi: 10.3390/en11071716.
[33] T. Lipo, *Analysis of Synchronous Machines*, 2nd ed. Boca Raton, FL, USA: CRC Press, 2012, pp. 1–6.
[34] S. Li, W. Li, J. Deng, T. D. Nguyen, and C. C. Mi, "A double-sided LCC compensation network and its tuning method for wireless power transfer," *IEEE Trans. Veh. Technol.*, vol. 64, no. 6, pp. 2261–2273, Jun. 2015.
[35] T. Campi, S. Cruciani, F. Maradei, and M. Feliziani, "Magnetic field during wireless charging in an electric vehicle according to standard SAE J2954," *Energies*, vol. 12, 2019, Art. no. 1795.

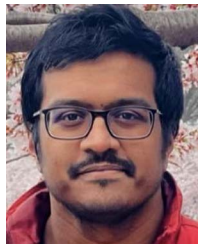

Samir Chowdhury (Member, IEEE) received the B.Sc. degree in electrical and electronic engineering from the Bangladesh University of Engineering and Technology, Dhaka, Bangladesh, in 2015, and the M.Sc. degree in electrical engineering from the University of Akron, Akron, OH, USA, in 2020.

He is currently a Power Electronics Engineer with EnerSys Delaware, Inc., Reading, PA, USA. His research interests include power electronic converter topologies, wireless charging, and high-frequency magnetics design.

Md Tawhid Bin Tarek (Student Member, IEEE) received the B.Sc. degree in electrical and electronic engineering from the Bangladesh University of Engineering and Technology, Dhaka, Bangladesh, in 2009, and the M.Sc. degree in electrical engineering in 2017 from The University of Akron, Akron, OH, USA, where he is currently working toward the Ph.D. degree in electrical engineering.

He is currently an Electric Motor Development Engineer with Techtronic Industries Limited, Hong Kong. His research interests include the design and control of electric motors.

Md Ehsanul Haque (Member, IEEE) received the B.S. degree in electrical and electronic engineering from the Bangladesh University of Engineering and Technology, Dhaka, Bangladesh, in 2014, and the Ph.D. degree in electrical engineering with a focus on power electronics and motor drives from The University of Akron, Akron, OH, USA, in 2022.

He is currently a Power Electronics Research Engineer with GE Global Research Center, Niskayuna, NY, USA. His research interests include power electronics topologies, high-power silicon carbide inverters for aircraft propulsion applications, and electromagnetic interference mitigations.

Yilmaz Sozer (Fellow, IEEE) received the B.S. degree in electrical engineering from the Middle East Technical University, Ankara, Turkey, and the M.S. and Ph.D. degrees in electric power engineering from Rensselaer Polytechnic Institute, Troy, NY, USA.

He is currently a Distinguished Professor with the Electrical and Computer Engineering Department and the Director of the Center for Advanced Vehicle and Energy Systems with The University of Akron, Akron, OH, USA. Before joining The University of Akron, he was with the Advanced Energy Conversion, Schenectady, NY, USA. His research interests include the design, control, and modeling of electrical drives, alternative energy systems, high-power isolated dc–dc converter systems, and static power conversion systems that interface energy storage and distributed generation sources with the electric utility.

Dr. Sozer is currently an Editor for the IEEE JOURNAL OF EMERGING AND SELECTED TOPICS IN POWER ELECTRONICS. He was an Associate Editor and the Paper Review Chair for the IEEE TRANSACTIONS ON INDUSTRY APPLICATIONS, and an Associate Editor for the IEEE TRANSACTIONS ON POWER ELECTRONICS. He is the past Chair of the IEEE IAS Renewable and Sustainable Energy Conversion Systems Committee.